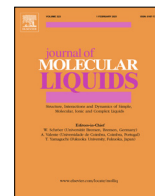




Since January 2020 Elsevier has created a COVID-19 resource centre with free information in English and Mandarin on the novel coronavirus COVID-19. The COVID-19 resource centre is hosted on Elsevier Connect, the company's public news and information website.

Elsevier hereby grants permission to make all its COVID-19-related research that is available on the COVID-19 resource centre - including this research content - immediately available in PubMed Central and other publicly funded repositories, such as the WHO COVID database with rights for unrestricted research re-use and analyses in any form or by any means with acknowledgement of the original source. These permissions are granted for free by Elsevier for as long as the COVID-19 resource centre remains active.



In-silico study for the screening and preparation of ionic liquid-AVDs conjugate to combat COVID-19 surge



Juhi Saraswat^a, Ufana Riaz^b, Rajan Patel^{a,*}

^aBiophysical Chemistry Laboratory, Centre for Interdisciplinary Research in Basic Sciences, Jamia Millia Islamia, New Delhi 110025, India

^bDepartment of Chemistry, Jamia Millia Islamia, New Delhi 110025, India

ARTICLE INFO

Article history:

Received 6 February 2022

Revised 13 April 2022

Accepted 26 April 2022

Available online 3 May 2022

Keywords:

Antiviral drugs

Ionic liquids

Conjugates

DFT

COVID-19

MD simulation

ABSTRACT

The pandemic due to COVID-19 caused by SARS-CoV-2 has led to the recorded deaths worldwide and is still a matter of concern for scientists to find an effective counteragent. The combination therapy is always been a successful attempt in treating various threatful diseases. Recently, Ionic liquids (ILs) are known for their antiviral activity. Fascinating tunable properties of ILs make them a potential candidate for designing the therapeutic agent. The concern while using ILs in biomedical field remains is toxicity therefore, choline-based ILs were used in the study as they are considered to be greener as compared to other ILs. In the present study strategically, we performed the blind molecular docking of antiviral drug (Abacavir, Acyclovir, and Galidesivir)-choline based ILs conjugates with the target protein (M_{pro} protease). The molecules were screened on the basis of binding energy. The data suggested that the combination of AVDs-ILs have greater antiviral potential as compared to the drugs and ILs alone. Further, the ADME properties and toxicity analysis of the screened conjugates was done which revealed the non-toxicity of the conjugates. Additionally, the energetic profiling of the ILs drugs and their conjugates was done using DFT calculations which revealed the stability of the conjugates and have a better option to be developed as a therapeutic agent. Also, from molecular dynamic simulation was done and results showed the stability of the complex formed between target protein and the designed conjugates of AVDs and ILs.

© 2022 Elsevier B.V. All rights reserved.

1. Introduction

It's been almost year and half, the outbreak of severe acute respiratory syndrome is still uncontrolled rather the situation in some part of the world has become even worst specially in the Asian countries [1]. As per the World Health Organisation, 1,49,432,808 coronavirus (COVID-19) cases have been recorded (on 8th June 2021, while writing the manuscript) and is expected to increase more intensively and exponentially by the end of the May 2021. The total death recorded till now is 34,49,189 worldwide however, 127,111,632 have been recovered [2]. The high mortality and morbidity are been seen in this pandemic due to coronavirus spread and is even more in 2021 as compared to 2019–20. The destruction is comparatively high as compared to the 2019–20. The reason being the continuous change of virus mutation which is more devastating than 2019–20 [3]. As previously reported, the spread of infection from host mediates via respiratory droplets, smog and fomites [4]. Structurally, the coronavirus is a single stranded RNA

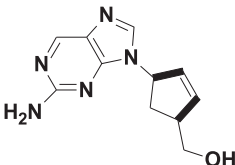
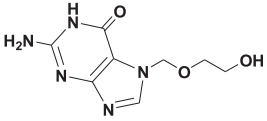
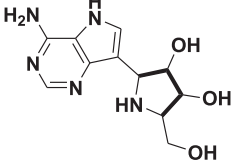
which directly affects the lungs and causes the lethal impact. The mechanism of action of the spike protein is already been discussed in our earlier publication [5]. Recently, in the March 2021 (Phase 2) in India National Centre for Disease Control (NCDC) reported that corona test carried out in Maharashtra, Delhi and Punjab showed new variant of coronavirus [6]. When genome sequencing was done by Indian SARS-CoV-2 Consortium on Genomics (INSACOG) it was found two important mutations in single variant and is termed as "double mutant" [7]. The rapid growth of this variant caused large destruction in India and still the panic situation continues and this clearly indicates the role of this variant in India's surge and the destruction is even far more as compared to first wave of corona infection in the year 2020 [8]. Other reason of India's surge could be the people lowered the guards and did not follow the COVID-19 protocol after the first wave. Opening of every sector to pre-covid level and inappropriate behaviour which was no longer taking care of the adverse effect exposed the susceptible population in a very big way [9].

Although we are in a mid of era where, urgent need of effective treatment is urgently needed. The whole world's scientist and doctors are working to find the way and stop the pandemic situation.

* Corresponding author.

E-mail address: rpatel@jmi.ac.in (R. Patel).

Table 1
Antiviral drugs (clinically tested) used in the computational trial for SARS-CoV-2.

S. no.	Antiviral Drugs	Chemical Structure	Biological activity	Mode of action
1.	Abacavir		Nucleoside reverse transcriptase inhibitor	Abacavir converts into carbovir triphosphate, lacks a 3'-OH group in DNA leading to chain termination.
2.	Acyclovir		Inhibit viral RNA or DNA polymerases	Acyclovir gets converted to acyclovir-triphosphate which competitively inhibit viral DNA polymerase
3.	Galidesivir		Inhibitor of RNA-polymerase	Binds to viral RNA and stops translation

India has developed the coronavirus drug named, Covid shield, Covaxin and a Russian drug, Sputnik-V have emerged as a hope to combat the battle against coronavirus [10,11]. Many other trials are in a pipeline to find the way out; however, still urgent drug development is needed. In our previous work we explored the antiviral potential of ILs against Covid-19 computationally [5]. The combination therapy is always been a successful attempt in treating various threatful diseases. Therefore, in the present work we aimed to create the combination of ILs and conventional antiviral drugs against a key regulator of the life cycle of coronavirus, main protease (M_{pro} or $3CL_{pro}$) enzyme [12]. M_{pro} plays a crucial role in the replication of the coronavirus as it promotes the translation of viral RNA to viral protein and causes a growth of coronavirus infection [13]. Hence, study on M_{pro} enzyme becomes an important drug target to study on to combat covid-19 surge [14]. ILs are the molten salts below 100 °C and composed of organic cation and organic/inorganic anions. ILs are known as designer solvents because of their tunable characteristic feature [15–17]. Though, the toxicity of ILs always has been a topic of concern for the researchers specially when designing the drug molecule. In this regard, we have chosen choline based-ILs in our study because of their greener property as well as low toxicity [18]. Recent studies showed the antiviral application of the ILs [19]. Palanisamy *et al.* in their work showed that ILs enhance the stability of M_{pro} protein and have significant contributions to the protein-drug binding, which may be useful in drug development for COVID-19. [20,21]. After extensive literature survey, we have computationally screened some choline based-ILs and antiviral drugs (abacavir, acyclovir, galidesivir) that are clinically tested (chemical structures given on Table 1). Also, the toxicity and drug likeliness assay were performed computationally to further filter out our findings for their application as a potential inhibitor of M_{pro} . Moreover, the density functional theory (DFT) was employed to determine the stability of IL_AVDS conjugates. With employing these advanced computational approaches, designed compounds might help in significant improvement in the antiviral activity and can have a better chance to be developed as drug leads against covid-19 virus.

2. Methods

Computation approach for designing a molecule plays an important role in developing the effective molecule against target molecules which causes severe illness. One of them nowadays

everybody countering with is Covid-19 disease. Repeated experiments and trials in laboratories and failures in the study is always been a problematic situation for the scientist working hard to combat in the pandemic situation. To overcome the chances of failure, computational approach plays an important role in biomedical field.

2.1. COVID-19 receptor molecule preparation

M_{pro} protease is reported as a regulatory enzyme important role in coronavirus infection and its progression in the body [22]. The three-dimensional structure of M_{pro} protease was obtained from protein data bank (PDB) (PDB ID: 6Y84) from <https://www.rcsb.org/> [5]. To study the effect of ILs as well as its conjugates with clinically tested antiviral drugs the computational study was done on M_{pro} protease.

2.2. Ligand preparation

We have taken Abacavir (ABA), Acyclovir (ACY), and Galidesivir (GAL) as antiviral drugs (AVDs) which was found to be active against covid-19 [23–25]. The biological importance and action of selected AVDs are listed in Table 1. In our previous studies ILs were found to be antiviral and toxicity remained an issue therefore Choline based ILs because of their green characteristic feature is found to be a potential candidate for the present study [26]. AVDs, choline-based-ILs namely *N*-(2-hydroxyethyl)-*N,N*-dimethylbutan-1-aminium, *N*-(2-hydroxyethyl)-*N,N*-dimethylhexan-1-aminium, *N*-(2-hydroxyethyl)-*N,N*-dimethyloctan-1-aminium, *N*-(2-hydroxyethyl)-*N,N*-dimethyldecan-1-aminium, and its conjugates with AVDs was drawn using ChemDraw 12.0 software and were saved as pdb format. The energy minimisation of all the structure was done using spdv.exe 4.10 software.

2.3. Molecular docking

The binding affinity of ILs, AVDs and IL-AVD conjugates towards M_{pro} protease was evaluated using AutoDock 1.5.6 software. The structure of the protein was optimised, water molecules were removed from the protein structure, polar hydrogen was added followed by the addition of AD4 type atoms to the protein. In the

same manner for the ligand's energy optimization was done. Lamarckian Genetic Algorithm embedded in AutoDock software was employed to evaluate the binding score of ligand protein interactions. The blind docking was performed, the protein and ligands was confined into the grid box in all axes which could accommodate the active site. The grid parameters are listed in Table S1. Thereafter, a total of 100 runs were set in the software to carry out the docking. After successful completion of all the docking

steps, the obtained conformers were ranked depending upon the highest binding energy value from molecular docking results.

2.4. Visualisation

The obtained results from molecular docking were further analysed using visualisation software. Depending upon the highest binding affinity score the stable conformer was selected and was

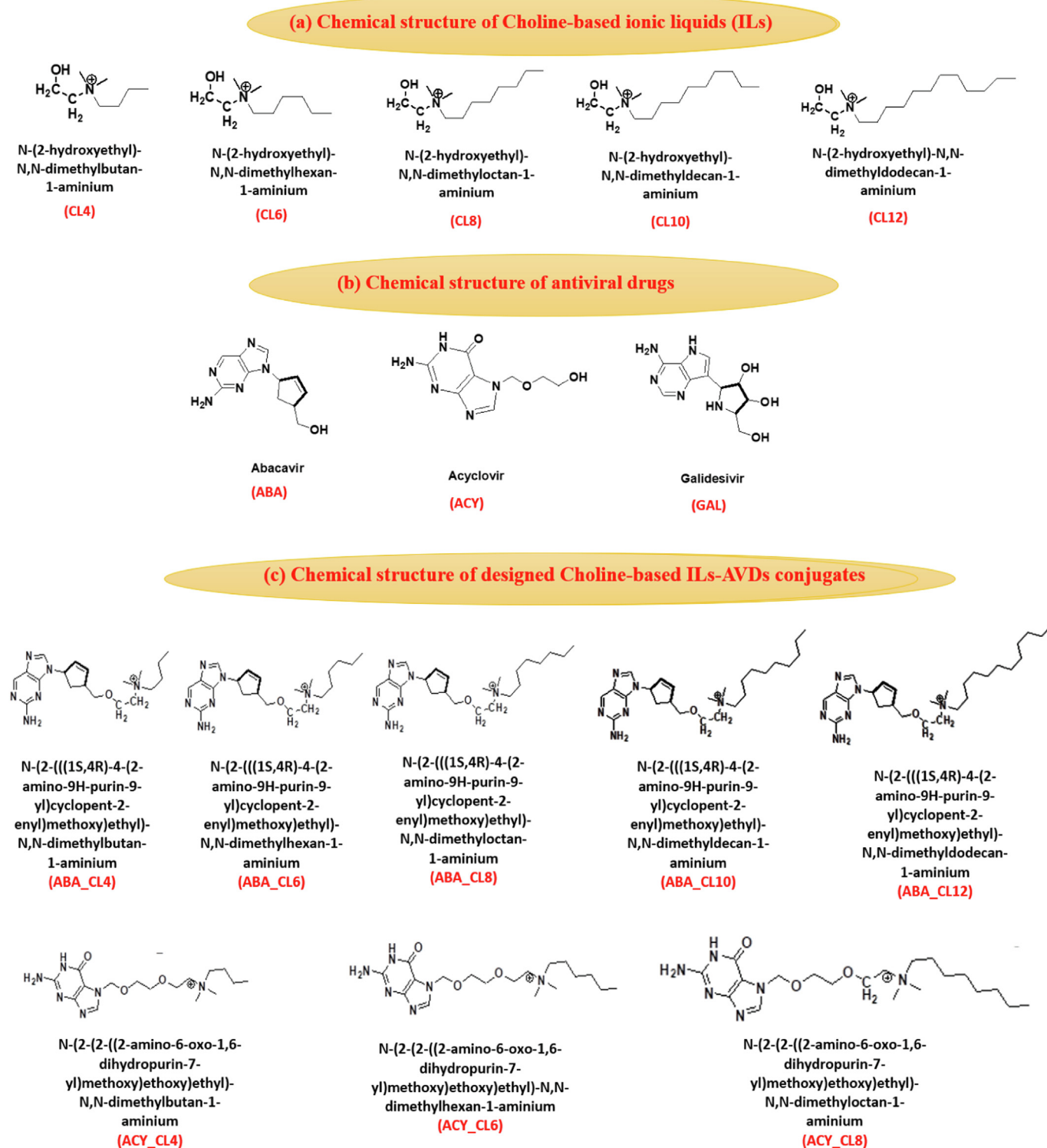


Fig. 1. Chemical structures of (a) Choline-based ILs (b) antiviral drugs (c) designed conjugates using ILs and AVDs.

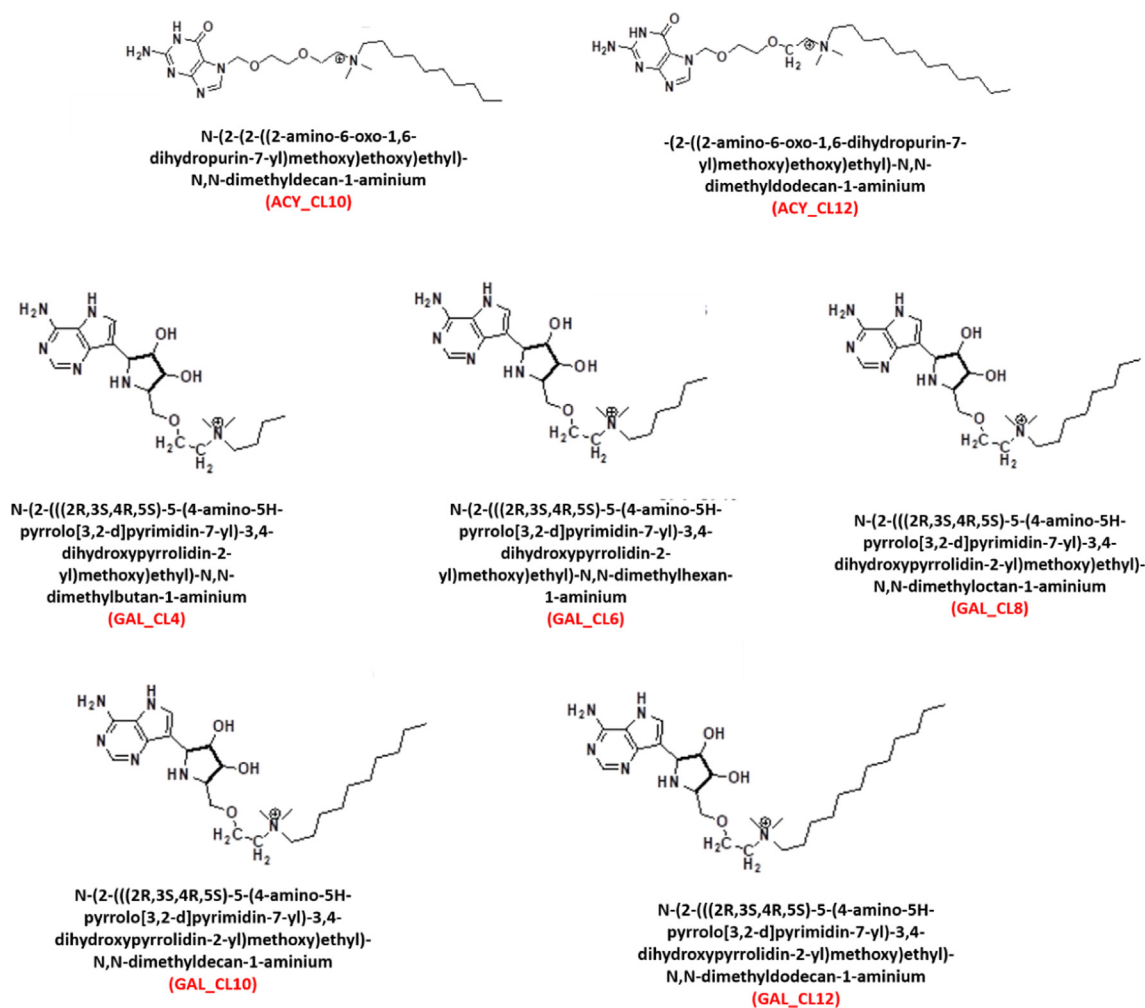


Fig. 1 (continued)

visualised using PyMol software. The 3D view of selected conformer and interaction involved (with bond length) between ligand and protein, UCSF Chimera 1.2 software was employed [5]. Additionally, the 2D view of most appropriate conformer was obtained using Discovery studio software (BIOVIA-2016) [15].

2.5. ADME analysis

Pharmacokinetics properties helps in predicting the safety and effectiveness of therapeutic agent taken in the study in the initial stages of drug discovery or development. The pharmacokinetics properties of therapeutic agent involve adsorption, distribution, metabolism and excretion of compound in the body. Freely available software SwissADME at <http://www.swissadme.ch/index.php> was used to predicts the pharmacokinetics of designed molecules (as shown in Fig. 1) [27].

2.6. Toxicity analysis

Toxicity of therapeutic agent in drug discovery is always been a matter of concern for the science fraternity. The computational approach for the prediction of toxicity of compounds plays a key role in the studies done for drug discovery. The toxicity profiling includes various parameters such as hepatotoxicity, immunogenicity, mutagenicity, carcinogenicity, etc. The selected compounds

(shown in Fig. 1) were screened for their toxicity profiling using a freely available software named software at <http://tox.charite.de/tox> [28].

2.7. Density functional theory (DFT)

DFT was employed to study the interaction occurring between ILs and AVDs. The best fit molecules were screened out on the basis of minimum binding energy obtained from molecular docking study and DFT calculations were done for the screened molecules. We used Gaussian 03 W for performing the DFT calculation and the Gaussian view was used to for optimization + frequency of the molecules. The tools set for DFT was B3LYP, 6-31G (d) basic set, +. Various Physiochemical descriptors viz. global electrophilicity index (ω), electronegativity (χ), chemical potential (μ), softness (S), and chemical hardness (η) of IL, drug and their complex, IL-drug were determined using Eqs. (1)–(5).

$$\mu = (E_{\text{HOMO}} + E_{\text{LUMO}})/2 \quad (1)$$

$$\chi = -(E_{\text{HOMO}} + E_{\text{LUMO}})/2 \quad (2)$$

$$\eta = (E_{\text{LUMO}} - E_{\text{HOMO}})/2 \quad (3)$$

$$S = (1/2\eta) \quad (4)$$

$$\omega = \left(\frac{\mu^2}{2\eta}\right) \quad (5)$$

$$\Delta E = E_{IL} + E_{ABA} - E_{(IL + ABA)}$$

2.8. Molecular dynamic simulation

MD simulation of the best screened molecule with target protein using Webgro and CABS-flex ver 2.0 [29, 30]. The stability of the complex was determined using the two parameters, root mean square deviation (RMSD) and root mean square fluctuation (RMSF). Webgro server was used to determine the RMSD value of the complex between target protein and ABA_CL12. Firstly, the topology for the best fit model of docked protein–ligand file was prepared for performing MD simulation using GROMOS96 43a1 forcefield. Topology of ligand file was generated using the freely available software, PRODRUG [31]. SPC was selected as solvent model for MD and the triclinic box of dimension 32x48x48 for the complex. Based on total charge sodium and chloride ions were added for neutralization. For energy minimization, steepest descent algorithm at 5000 steps was set. The MD simulation was carried out at NVT/NTP conditions (300 K, 1 bar) in presence of 0.15 M NaCl. The number of frames per simulation was set at 1000. The simulation time for MD was set at 100 ns and numbers of cycles were set to 50. Rest all parameters were left as default [32].

3. Results

3.1. Molecular Docking analysis

Molecular docking of three antiviral drugs, ABA, ACY, and GAL and their conjugates with choline-based ILs was done to evaluate the enhanced antiviral potential of the designed conjugates against SARS-CoV-2 protease using AutoDock tool as mentioned in section 2.3. Molecular docking results obtained were analysed and obtained conformers after docking were ranked depending up on

the minimum binding energy and the best fit conformer was selected in each case system. The obtained binding energy values through molecular docking are listed in Table 2.

3.2. Molecular docking of ILs

Molecular docking results of five choline-based ILs are summarized in Table 2. Most favourable conformer (2D and 3D figures) of docked pose of all five-choline based ILs are shown in Fig. 2. The docked images clearly depicts that the binding of ILs at the active site of SARS-CoV-2 protease. Fig. 2I (a) show that CL4 binds firmly with the target protein. Residues, Lys-5, Arg-131, Thr-199, Leu-286 in target protein were involved in the interaction through van der waal with CL4. Besides, Glu-288, Asp-289, Glu-290 residues showed the attractive charge interaction with CL4. Leu-287 showed a carbon-hydrogen interaction between target protein and CL4 as shown in Fig. 2I(b). The binding energy obtained was -3.97 kcal/mol.

Similarly, Fig. 2II(a) shows the docked pose of CL6 with target protein. Figure shows that CL6 binds firmly with the target protein. Residues, Phe-140, Asn-142, His-163, His-164, Met-165, and His-172 in target protein were involved in the interaction through van der waal with CL6. Besides, Leu-141, Ser-144, and Cys-145 residues showed the conventional hydrogen interaction with CL6. His-41, and Met-49 showed a pi-sigma interaction with CL6. Glu-166 showed the attractive charge interaction with CL6 and Gly-148 on target protein showed the donor–donor interaction with CL6 as shown in Fig. 2II(b). The binding energy obtained was -4.61 kcal/mol. Fig. 2III(a) shows the docked pose of CL8 with target protein. Figure shows that CL8 binds firmly with the target protein. Residues, Gln-127, Cys-128, Lys-137, and Leu-286 in target protein were involved in the interaction through van der waal with CL8. Besides, Lys-5 residues showed the conventional hydrogen interaction with CL8. Glu-288, Asp-289, and Glu-290 showed the attractive charge interaction with CL8 as shown in Fig. 2III(b). The binding energy obtained was -5.01 kcal/mol.

Table 2

Binding energy (kcal/mol) of the potential inhibitors of Sars-CoV-2 obtained from molecular docking analysis.

S. no.	System	IUPAC names	Binding energy (kcal/mol)
	CL4	N-(2-hydroxyethyl)-N,N-dimethylbutan-1-aminium	-3.97
	CL6	N-(2-hydroxyethyl)-N,N-dimethylhexan-1-aminium	-4.61
	CL8	N-(2-hydroxyethyl)-N,N-dimethyloctan-1-aminium	-5.01
	CL10	N-(2-hydroxyethyl)-N,N-dimethyldecane-1-aminium	-5.05
	CL12	N-(2-hydroxyethyl)-N,N-dimethyldodecan-1-aminium	-5.91
	Abacavir	((1S,4R)-4-(2-amino-9H-purin-9-yl)cyclopent-2-enyl)methanol	-6.91
	ABA_CL4	N-(2-(((1S,4R)-4-(2-amino-9H-purin-9-yl)cyclopent-2-enyl)methoxy)ethyl)-N,N-dimethylbutan-1-aminium	-5.78
	ABA_CL6	N-(2-(((1S,4R)-4-(2-amino-9H-purin-9-yl)cyclopent-2-enyl)methoxy)ethyl)-N,N-dimethylhexan-1-aminium	-6.28
	ABA_CL8	N-(2-(((1S,4R)-4-(2-amino-9H-purin-9-yl)cyclopent-2-enyl)methoxy)ethyl)-N,N-dimethyloctan-1-aminium	-7.01
	ABA_CL10	N-(2-(((1S,4R)-4-(2-amino-9H-purin-9-yl)cyclopent-2-enyl)methoxy)ethyl)-N,N-dimethyldecane-1-aminium	-7.12
	ABA_CL12	N-(2-(((1S,4R)-4-(2-amino-9H-purin-9-yl)cyclopent-2-enyl)methoxy)ethyl)-N,N-dimethyldodecan-1-aminium	-8.13
	Acyclovir	2-amino-7-((2-hydroxyethoxy)methyl)-1H-purin-6(7H)-one	-5.72
	ACY_CL4	N-(2-(2-((2-amino-6-oxo-1,6-dihydropurin-7-yl)methoxy)ethoxy)ethyl)-N,N-dimethylbutan-1-aminium	-5.03
	ACY_CL6	N-(2-(2-((2-amino-6-oxo-1,6-dihydropurin-7-yl)methoxy)ethoxy)ethyl)-N,N-dimethylhexan-1-aminium	-5.6
	ACY_CL8	N-(2-(2-((2-amino-6-oxo-1,6-dihydropurin-7-yl)methoxy)ethoxy)ethyl)-N,N-dimethyloctan-1-aminium	-6.13
	ACY_CL10	N-(2-(2-((2-amino-6-oxo-1,6-dihydropurin-7-yl)methoxy)ethoxy)ethyl)-N,N-dimethyldecane-1-aminium	-6.28
	ACY_CL12	N-(2-(2-((2-amino-6-oxo-1,6-dihydropurin-7-yl)methoxy)ethoxy)ethyl)-N,N-dimethyldodecan-1-aminium	-6.45
	Galidesivir	(2S,3R,4S,5R)-2-(4-amino-5H-pyrrolo[3,2-d]pyrimidin-7-yl)-5-(hydroxymethyl)pyrrolidine-3,4-diol	-6.34
	GLA_CL4	N-(2-(((2R,3S,4R,5S)-5-(4-amino-5H-pyrrolo[3,2-d]pyrimidin-7-yl)-3,4-dihydroxypyrrrolidin-2-yl)methoxy)ethyl)-N,N-dimethylbutan-1-aminium	-4.25
	GLA_CL6	N-(2-(((2R,3S,4R,5S)-5-(4-amino-5H-pyrrolo[3,2-d]pyrimidin-7-yl)-3,4-dihydroxypyrrrolidin-2-yl)methoxy)ethyl)-N,N-dimethylhexan-1-aminium	-4.72
	GLA_CL8	N-(2-(((2R,3S,4R,5S)-5-(4-amino-5H-pyrrolo[3,2-d]pyrimidin-7-yl)-3,4-dihydroxypyrrrolidin-2-yl)methoxy)ethyl)-N,N-dimethyloctan-1-aminium	-5.81
	GLA_CL10	N-(2-(((2R,3S,4R,5S)-5-(4-amino-5H-pyrrolo[3,2-d]pyrimidin-7-yl)-3,4-dihydroxypyrrrolidin-2-yl)methoxy)ethyl)-N,N-dimethyldecane-1-aminium	-6.18
	GLA_CL12	N-(2-(((2R,3S,4R,5S)-5-(4-amino-5H-pyrrolo[3,2-d]pyrimidin-7-yl)-3,4-dihydroxypyrrrolidin-2-yl)methoxy)ethyl)-N,N-dimethyldodecan-1-aminium	-6.75

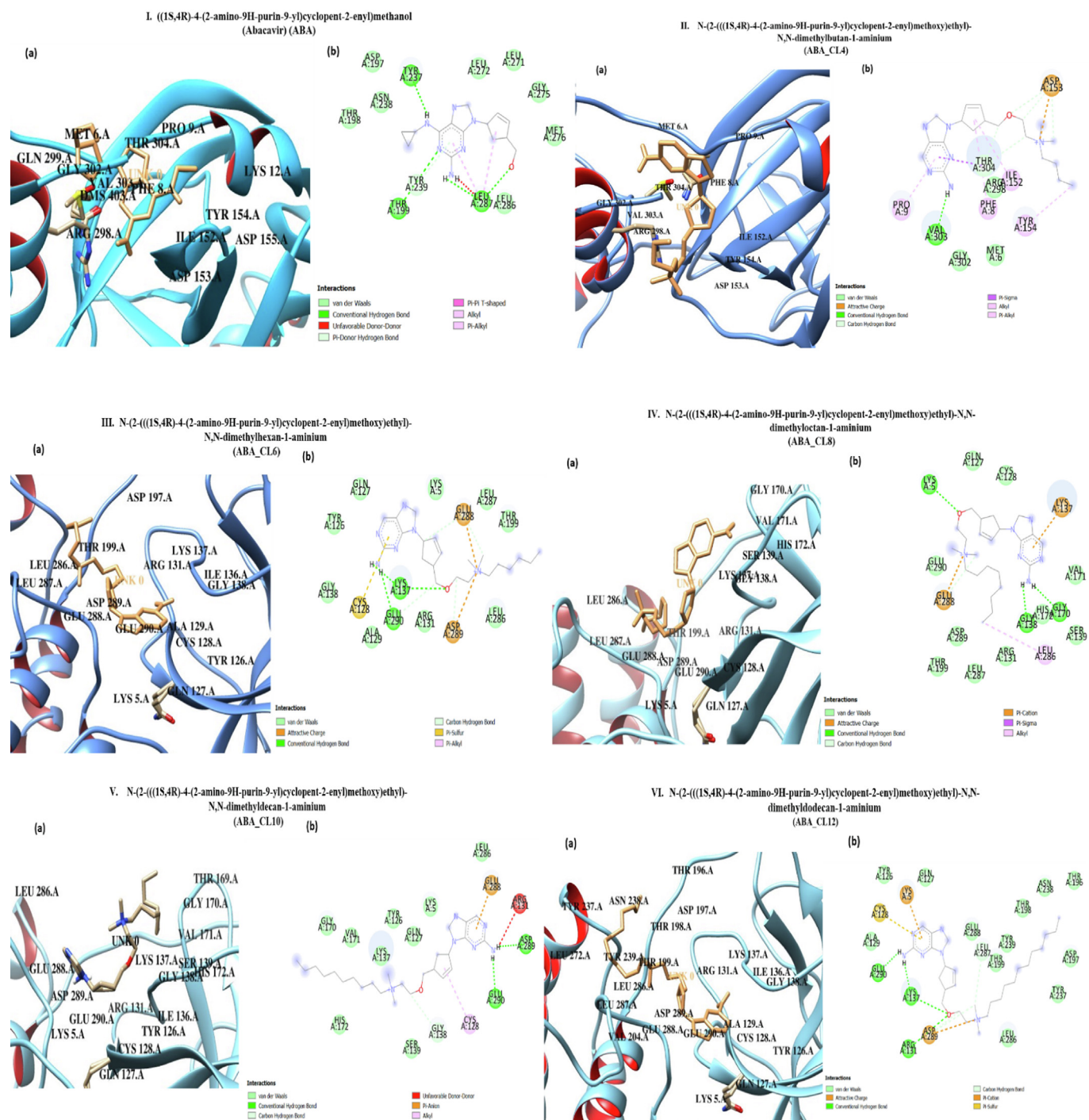


Fig. 2. Representation 3D (a) and 2D (b) of (I)ABA (II) ABA_CL4 (III) ABA_CL6 (IV) ABA_CL8 (V) ABA_CL10 (VI) ABA_CL12 docked M_{pro} protease.

Fig. 2IV(a) shows the docked pose of CL10 with target protein. Figure shows that CL10 binds firmly with the target protein. Residues, Lys-5, Tyr-126, Gln-127, Cys-128, Gly-138, Ser-139, and Leu-286 in target protein were involved in the interaction through van der waal with CL10. Besides, Lys-137 residue showed the conventional hydrogen interaction with CL10. Glu-288, Asp-289, and Glu-290 showed the attractive charge interaction with CL10 and Arg-131 on target protein showed the donor-donor interaction with CL10 as shown in Fig. 2IV(b). The binding energy obtained was -5.05 kcal/mol. Fig. 2V(a) shows the docked pose of CL12 with target protein. Figure shows that CL12 binds firmly with the target protein. Residues, Asp-197, Leu-286, Leu-287, Asn-238, Tyr-237,

Thr-198, Thr-199, and Arg-131 in target protein were involved in the interaction through van der waal with CL12. Besides, Lys-5 residue showed the conventional hydrogen interaction with CL12. Glu-288, Asp-289, and Glu-290 showed the attractive charge interaction with CL12 as shown in Fig. 2V(b). The binding energy obtained was -5.91 kcal/mol. From Table 2 it can be seen that with increasing the alkyl chain length the value of binding energy decreases. CL12 showed minimum binding energy with target protein which depicts that with increasing carbon chain length at N-atom the antiviral activity of the IL increase and becomes more potent against novel coronavirus. Our results comply with the results we achieved where it was clearly seen that with increasing

hydrophobicity the antimicrobial characteristic of the corresponding IL increases.

3.3. Molecular docking of antiviral drugs (AVDs)

Molecular docking results of five choline-based ILs with M_{pro} protease (target protein) are summarized in Table 2. Most favourable conformer (2D and 3D figures) of docked pose of selected

antiviral drugs (chemical structures are given in figure) are shown in Fig. 3I, 4I, 5I. The docked images clearly depicts that the binding of drugs, ABA, ACY, and GAL binds at the active site of SARS-CoV-2 protease. Fig. 3I shows that ABA binds firmly with the target protein. Residues, ASP-197, THR-198, ASN-238, TYR-239, LEU-271, LEU-272, GLU-275, MET-276, LEU-286 in target protein were involved in the interaction through van der waal with ABA. Besides, THR-199, TYR-237, LEU-287 residues showed a conven-

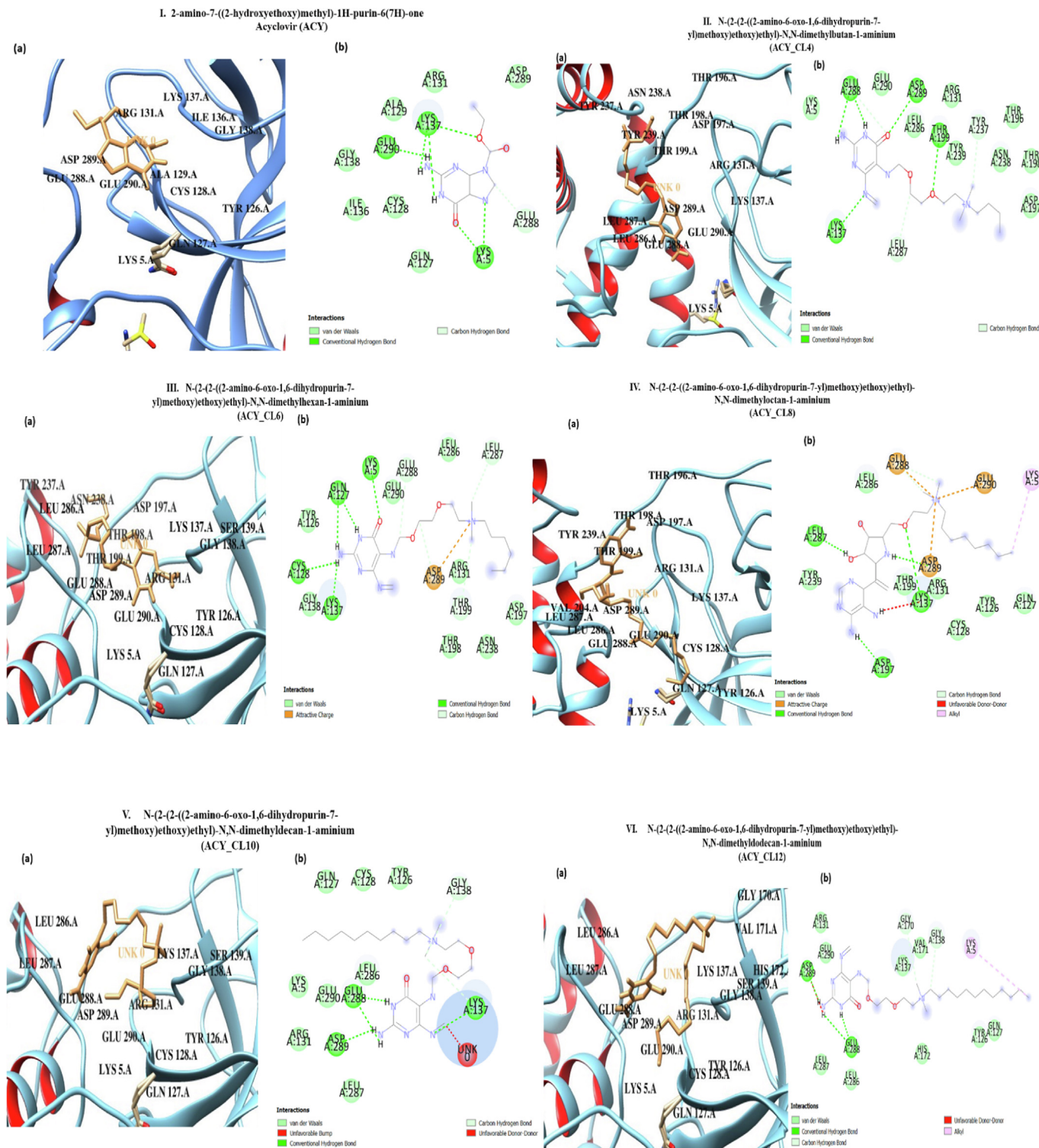


Fig. 3. Representation 3D (a) and 2D (b) of (I) ACY (II) ACY_CL4 (III) ACY_CL6 (IV) ACY_CL8 (V) ACY_CL10 (VI) ACY_CL12 docked M_{pro} protease.

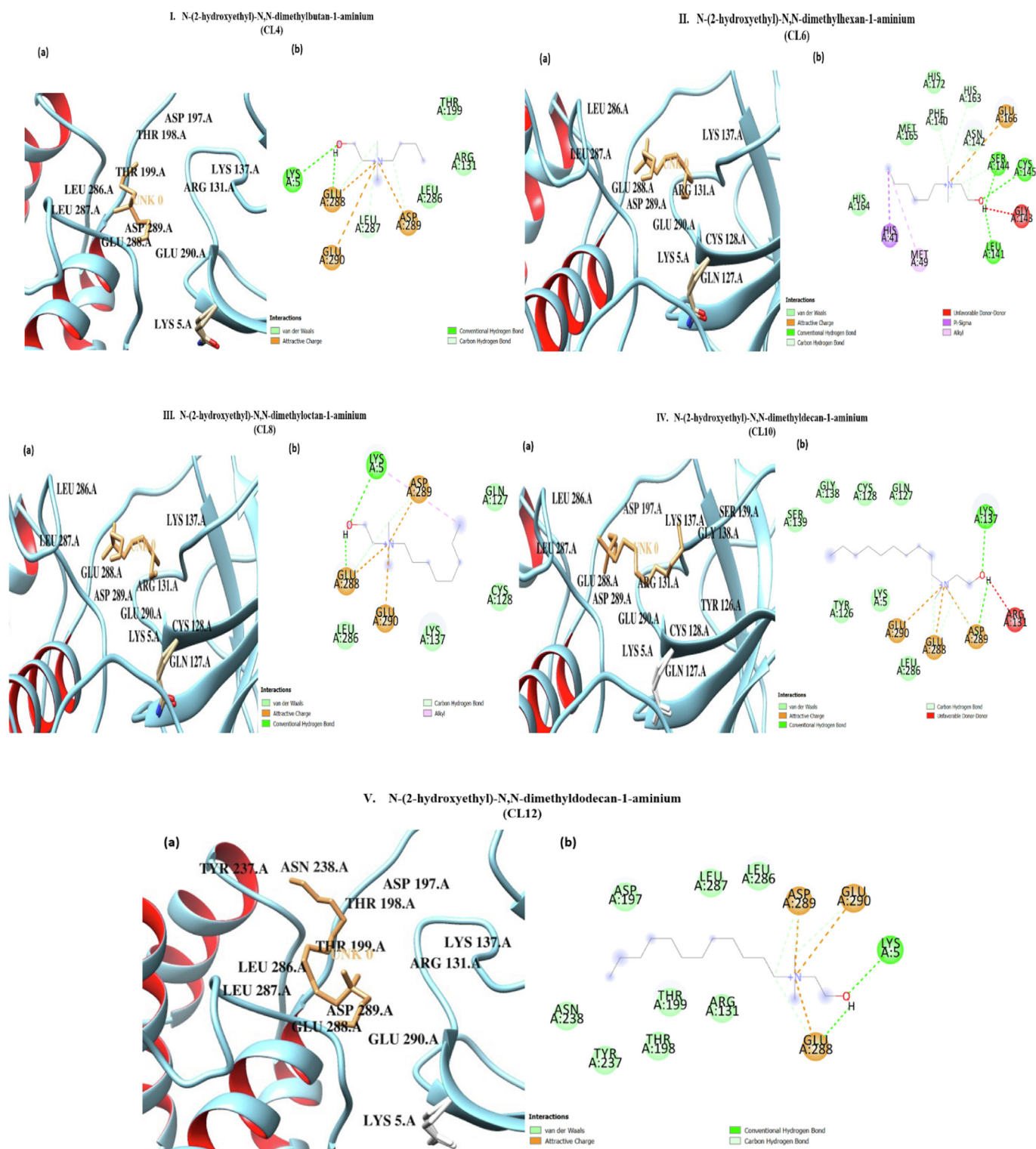


Fig. 5. Representation 3D (a) and 2D (b) of (I) CL4 (II) CL6 (III) CL8 (IV) CL10 (V) CL12 docked M_{pro} protease.

conjugates (ABA_CL4, ABA_CL6, ABA_CL8, ABA_CL10, ABA_CL12) (chemical structures are given in Fig. 1(c)) are shown in Fig. 3III-VI. The docked images clearly depicts that the binding of drugs binds at the active site of SARS-CoV-2 protease. Fig. 3 shows that all five conjugates of ABA binds firmly with the target protein. The docked pose of ABA_CL4 (shown in Fig. 3II(a)) showed that the residues, Met-5, Arg-289, and Gly-302 in target protein were involved in the interaction through van der waal with ABA_CL4.

Besides, Val-303 residue showed a conventional hydrogen bond interaction with ABA_CL4. Thr-303 showed the carbon hydrogen bond interaction with ABA_CL4. Asp-153 showed the attractive charge interaction with ABA_CL4. Phe-8, Ile-152, Tyr-154 showed the pi-sigma interaction with ABA_CL4. Pro-9 residue showed the pi-alkyl interaction with ABA_CL4 as shown in Fig. 3II(b). The obtained binding energy was found to be -5.78 kcal/mol. The docked pose of ABA_CL6 (in Fig. 3III(a)) showed that the residues,

Lys-5 Tyr-126, Gln-127, Ala-129, Arg-131, Gly-138, Thr-199, Leu-286, and Leu-287 in target protein were involved in the interaction through van der waal with ABA_CL6. Besides, Lys-137, and Glu-290 residues showed a conventional hydrogen bond interaction with ABA_CL6. Cys-128, Glu-288, and Asp-289 showed the attractive charge interaction with ABA_CL6 as shown in Fig. 3III (b). The binding energy obtained was -6.28 kcal/mol. The docked pose of ABA_CL8 (in Fig. 3IV(a)) showed that the residues, Gln-127, Cys-128, Arg-131, Ser-139, Val-171, His-172, Thr-199, Leu-287, Asp-289, and Glu-290 in target protein were involved in the interaction through van der waal with ABA_CL8. Besides, Lys-5, Gly-138, and Gly-170 residues showed a conventional hydrogen bond interaction with ABA_CL8. Lys-137, and Glu-288 showed the attractive charge interaction with ABA_CL8. Leu-286 showed a pi-sigma interaction with ABA_CL8 as shown in Fig. 3IV(b). The binding energy obtained was -7.01 kcal/mol. The docked pose of ABA_CL10 as shown in Fig. 3V(a)) showed that the residues, Lys-5, Tyr-126, Gln-127, Lys-137, Gly-138, Ser-139, Gly-170, Val-171, and His-172 in target protein were involved in the interaction through van der waal with ABA_CL10. Besides, Asp-289, and Glu-290 and residues showed a conventional hydrogen bond interaction with ABA_CL10. Cys-128 showed the alkyl interaction with ABA_CL10. Glu-288 showed a pi-anion interaction with ABA_CL10. Arg-131 showed the donor-donor interaction with ABA_CL10 as shown in Fig. 3V(b). The binding energy obtained was -7.12 kcal/mol. The docked pose of ABA_CL12 (in Fig. 3VI(a)) showed that the residues, Tyr-126, Gln-127, Ala-129, Thr-196, Asp-197, Thr-198, Tyr-237, Asn-238, Tyr-239, Leu-286, Leu-287, and Glu-288 in target protein were involved in the interaction through van der waal with ABA_CL12. Besides, Arg-131, Lys-137, and Glu-290 residues showed a conventional hydrogen bond interaction with ABA_CL12. Lys-5, and Asp-289 showed the pi-cation interaction whereas, Cys-128 showed the pi-sulphur interaction with ABA_CL12 as shown in Fig. 3VI(b). The binding energy obtained was -8.13 kcal/mol. The overall results showed that the binding energy obtained for all the conjugates originating from ABA and choline-based ILs is higher as that of abacavir, signifies that they have increased antiviral potential as compared to the drug and also, individual IL. The maximum potential was obtained in case of ABA_CL12 (ILs having longer carbon chain).

Also, the antiviral activity of conjugates originating from ACY and choline based ILs were evaluated using molecular docking approach. Most favourable conformer (2D and 3D figures) of docked pose of designed conjugates (ACY_CL4, ACY_CL6, ACY_CL8, ACY_CL10, ACY_CL12) (chemical structures are given in Fig. 1(c)) are shown in Fig. 4 II-VI. The docked images clearly depicts that the binding of drugs at the active site of SARS-CoV-2 protease. The results showed that all five conjugates of ACY bind firmly with the target protein. The docked pose of ACY_CL4 (in Fig. 4II(a)) showed that the residues, Lys-5, Arg-131, Thr-196, Asp-197, Thr-198, Asn-238, Tyr-237, Tyr-239, Leu-286 Leu-287, and Glu-288 in target protein were involved in the interaction through van der waal with ACY_CL4. Besides, Lys-137, Thr-199, Glu-288, and Asp-289 residues showed a conventional hydrogen bond interaction with ABA_CL4. Lys-5 and Leu-287 residues carbon hydrogen bond interaction with ABA_CL4 as shown in Fig. 4II(b). The binding energy obtained was -5.03 kcal/mol. The docked pose of ACY_CL6 (Fig. 4III(a)) showed that the residues, Tyr-126, Arg-131, Gly-138, Asp-197, Thr-198, Thr-199, Asn-238, Leu-286, Leu-287, Glu-288, and Glu-290 in target protein were involved in the interaction through van der waal with ACY_CL6. Besides, Lys-5, Lys-137, Cys-128, Gln-127, Thr-199, Glu-288, and Asp-289 residues showed a conventional hydrogen bond interaction with ABA_CL6. Asp-289 residue showed attractive charge interaction with ACY_CL6 as shown in Fig. 4 III(b). The binding energy obtained was -5.60 kcal/mol.

The docked pose of ACY_CL8 (Fig. 4IV(a)) showed that the residues, Tyr-126, Gln-127, Cys-128, Arg-131, Thr-199, Tyr-239, and Leu-286 in target protein were involved in the interaction through van der waal with ACY_CL8. Besides, Lys-137, Leu-287, and Asp-197 residues showed a conventional hydrogen bond interaction with ACY_CL8. Glu-288, Asp-289, and Glu-290 residues showed attractive charge interaction with ACY_CL8 as shown in Fig. 4IV(b). The binding energy obtained was -6.13 kcal/mol. The docked pose of ACY_CL10 (Fig. 4V(a)) showed that the residues, Lys-5, Tyr-126, Gln-127, Cys-128, Arg-131, Gly-138, Glu-290, Leu-286, and Leu-287 in target protein were involved in the interaction through van der waal with ACY_CL10. Besides, Lys-137, Glu-288, and Asp-289 residues showed a conventional hydrogen bond interaction with ACY_CL10 as shown in Fig. 4V(b). The binding energy obtained was -6.28 kcal/mol. The docked pose of ACY_CL12 (Fig. 4VI(a)) showed that the residues, Arg-131, Glu-290, Lys-137, Gly-170, Val-171, Gly-138, Gln-127, Tyr-126, His-172, Leu-287, and Leu-286 in target protein were involved in the interaction through van der waal with ACY_CL12. Besides, Glu-288, and Asp-289 residues showed a conventional hydrogen bond interaction with ACY_CL12. Lys-5 residue showed the alkyl interaction with ACY_CL12 as shown in Fig. 4VI(b). The binding energy obtained was -6.45 kcal/mol.

The docked pose of GAL_CL4 (Fig. 5II(a)) showed that the residues, Ile-152, Phe-8, Phe-294, Thr-292, Val-104, Ile-106, and Thr-111 in target protein were involved in the interaction through van der waal with GAL_CL4. Besides, Gln-110, Asp-295, and Asn-151 residues showed a conventional hydrogen bond interaction with GAL_CL4. Asp-153 residue showed attractive charge interaction with GAL_CL4. Arg-298 showed the donor donor interaction with GAL_CL4 as shown in Fig. 5II(b). The binding energy obtained was -4.25 kcal/mol. The docked pose of GAL_CL6 (Fig. 5III(a)) showed that the residues, Tyr-126, Gln-127, Gly-138, Cys-128, Lys-137, Leu-287, and Leu-286 in target protein were involved in the interaction through van der waal with GAL_CL6. Besides, Glu-288, and Asp-289 residues showed a conventional hydrogen bond interaction with GAL_CL6. Lys-5 showed the alkyl interaction with GAL_CL6. Glu-290 residue showed attractive charge interaction with GAL_CL6 as shown in Fig. 5III(b). The binding energy obtained was -4.72 kcal/mol. The docked pose of GAL_CL8 (Fig. 5IV (a)) showed that the residues, Tyr-126, Gln-127, Cys-128, Arg-131, Thr-199, Tyr-239, and Leu-286 in target protein were involved in the interaction through van der waal with GAL_CL8. Besides, Lys-137, Leu-287, and Asp-197 residues showed a conventional hydrogen bond interaction with GAL_CL8. Glu-288, Asp-289, and Glu-290 residues showed attractive charge interaction with GAL_CL8. Lys-5 showed alkyl interaction with GAL_CL8 as shown in Fig. 5IV(b). The binding energy obtained was -5.81 kcal/mol. The docked pose of GAL_CL10 (Fig. 5V(a)) showed that the residues, Leu-286, Leu-287, Ala-129, Cys-128, Tyr-126, Ser-139, Gly-138, Lys-5, Asp-197, Thr-199, Thr-198, Arg-131 in target protein were involved in the interaction through van der waal with GAL_CL10. Besides, Gln-127 residue showed a conventional hydrogen bond interaction with GAL_CL10. Glu-290, Asp-289, Glu-288 residues showed the attractive charge interaction with GAL_CL10. Lys-137 showed the acceptor-acceptor interaction with GAL_CL10 as shown in Fig. 5V(b). The binding energy obtained was -6.18 kcal/mol. The docked pose of GAL_CL12 (Fig. 5VI(a)) showed that the residues, Tyr-126, Cys-128, Lys-5, Glu-288, Leu-286, Arg-131, Thr-135, Asp-169, Gly-170 Arg-131, Glu-290, Lys-137, Gly-170, Gly-138 in target protein were involved in the interaction through van der waal with GAL_CL12. Besides, Gln-127 residue showed a conventional hydrogen bond interaction with GAL_CL12. Val-171, Ala-194 residues showed alkyl interaction with GAL_CL12 as shown in Fig. 5VI(b). The binding energy obtained was -6.75 kcal/mol.

3.5. ADME

The pharmacokinetics features of therapeutic agent molecule such as adsorption, distribution, metabolism, and excretion are very important to be determined for the molecule to act as drug. The likeliness of any therapeutic agent/drug is given by Lipinski rule of five which includes certain range of parameters viz. molecular weight should be less than 500 Da, h-bond donor should be less than 5, H-bond acceptor must be less than 10, log P value should be less than 5 for a compound to be a candidate for drug development [33]. These parameters for selected class of compounds were calculated using SwizzAdme software as described in section 2.5. The values obtained for the above said parameters are listed in **Table S3**. The best fit molecules on the basis of minimum binding energy obtained from molecular docking was, ABA_CL12, ABA_CL10, ABA_CL8 and ABA. Amongst 23 compounds, the best fit molecule on the basis of binding energy was screened out and the results for best molecules are listed in **Table 3**. From **Table 3**, the binding energy of ABA_CL12, ABA_CL10, ABA_CL8 and ABA was found to be -8.13 , -7.12 , -7.01 , -6.91 kcal/mol, respectively. The value binding energy of screened conjugates was found to be much lower than that of conventional antiviral drug, ABA which suggests the high potency of the conjugates than that of antiviral drug. The ADME property describing parameters were found to be in range according to the reported literature. The logP value obtained for ABA_CL12, ABA_CL10, ABA_CL8 and ABA was 2.8, 2.3, 1.9, and -0.15 , respectively which was less than that of 5 suggesting the solubility of conjugates and drug in aqueous medium. The molecular weight of ABA_CL12, ABA_CL10, ABA_CL8 and ABA was found to be 471.7, 443.65, 415.6 and 231.25 Da, respectively which was lesser than that of a standard limit 500 Da⁵. The value of H-bond donor for ABA_CL12, ABA_CL10, ABA_CL8 and ABA was 1, 1, 1, 2, respectively and for H-bond acceptor the value was 4, 4, 4, and 4 respectively. The results revealed the drug likeliness of the conjugates [33].

3.6. Toxicity

Toxicity determination is a very crucial to be counted before designing any therapeutic agent. Therefore, the toxicity profile of all selected drugs/IL and designed conjugates were done using online available software as discussed in section 2.6. Various features such as blood brain barrier (BBB) penetration, GI adsorption,

CYP inhibitory promiscuity, and rat acute toxicity (LD50) value were obtained from software. The parameters obtained are listed in **Table S4**. Amongst 23 compounds, the best fit molecule on the basis of binding energy was screened out and the results for best molecules are listed in **Table 4**. From **Table 4**, the data suggests that the conjugates, ABA_CL12, ABA_CL10, ABA_CL8 showed high GI absorption but showed negative results for BBB which implies that the conjugates can't cross the blood brain barrier. CYP2D6, CYP3A4 is an important-enzymes found in liver and intestine. It helps in the oxidation of foreign organic molecule and supports in excretion[34]. Our results showed the inhibition of these enzymes in the presence of the conjugate whereas no inhibition of the important enzymes such as CYP1A2, CYP2C19, and CYP2C9 which further helps in the excretion of foreign molecule from the body. The LD50 value of all the studied compounds is summarized in **Table S4**. The value of LD50 decides the toxicity factor of any therapeutic agent [34]. According to the literature the LD50 range is classified into 4 categories. First in which $LD50 \leq 50$ mg/kg; second in which 50 mg/kg $< LD50 \leq 500$ mg/kg and are considered as toxic; third category in which 500 mg/kg $< LD50 \leq 5000$ mg/kg) and fourth category where, $LD50 > 5000$ mg/kg are considered to be non-toxic [5,35]. In our study the screen molecule falls under the category 3 and are considered to be non-toxic.

3.7. Density functional theory

To study the interaction between antiviral drug, ABA and ILs classical density functional theory (DFT) was employed. Optimized structures of ABA, CL8, CL10, CL12, ABA_CL8, ABA_CL10, ABA_CL12 and their HOMO and LUMO structures are shown in **Fig. 6**. Using equation 6, the energy difference (ΔE) was calculated to elucidate the feasibility of electron transfer between donor-acceptor of IL and drug and strength of interactions in the ABA-IL complexes. From **Fig. 6**, the optimized structures show the strong interaction of CL8, CL10 and CL12 with ABA. The energy of the optimized structures of ABA, CL8, CL10, CL12, ABA_CL8, ABA_CL10, and ABA_CL12 are -775.96 , -604.02 , -682.46 , -761.07 , -1303.52 , -1382.15 , and -1460.35 a.u. respectively. The energy difference of each complex is -76.46 , -76.28 , and -76.68 a.u., respectively. The obtained results suggest that the interaction between ABA and ILs are stable and cation-anion and anion induced dipole interactions are involved in gaseous phase. Ionization potential (IE) and electron affinity (EA) of a molecule or system is directly related to energy

Table 3

Prediction of molecular properties descriptors of the potential inhibitors of Sars-CoV-2 obtained from Swiss ADME analysis.

S. No.	Compounds	MW	Rotatable bonds	H-bond acceptors	H-bond donors	MLOGP	ESOL Solubility (mg/ml)	Solubility
1.	Abacavir	231.25	2	4	2	-0.15	6.77E + 00	Very soluble
2.	ABA_CL8	415.6	13	4	1	1.97	2.05E-02	Moderately soluble
3.	ABA_CL10	443.65	15	4	1	2.39	4.28E-03	Moderately soluble
4.	ABA_CL12	471.7	17	4	1	2.8	8.87E-04	Moderately soluble

Table 4

Toxicity Prediction of all studied compounds the potential inhibitors of Sars-CoV-2 obtained using ProTox-II prediction software.

Compounds	GI absorption	BBB permeant	CYP1A2 inhibitor	CYP2C19 inhibitor	CYP2C9 inhibitor	CYP2D6 inhibitor	CYP3A4 inhibitor	Predicted LD50 (mg/kg)	Predicted toxicity class
Abacavir	High	No	No	No	No	No	No	570	4
ABA_CL8	High	No	No	No	No	Yes	Yes	467	4
ABA_CL10	High	No	No	No	No	Yes	Yes	467	4
ABA_CL12	High	No	No	No	No	Yes	Yes	467	4

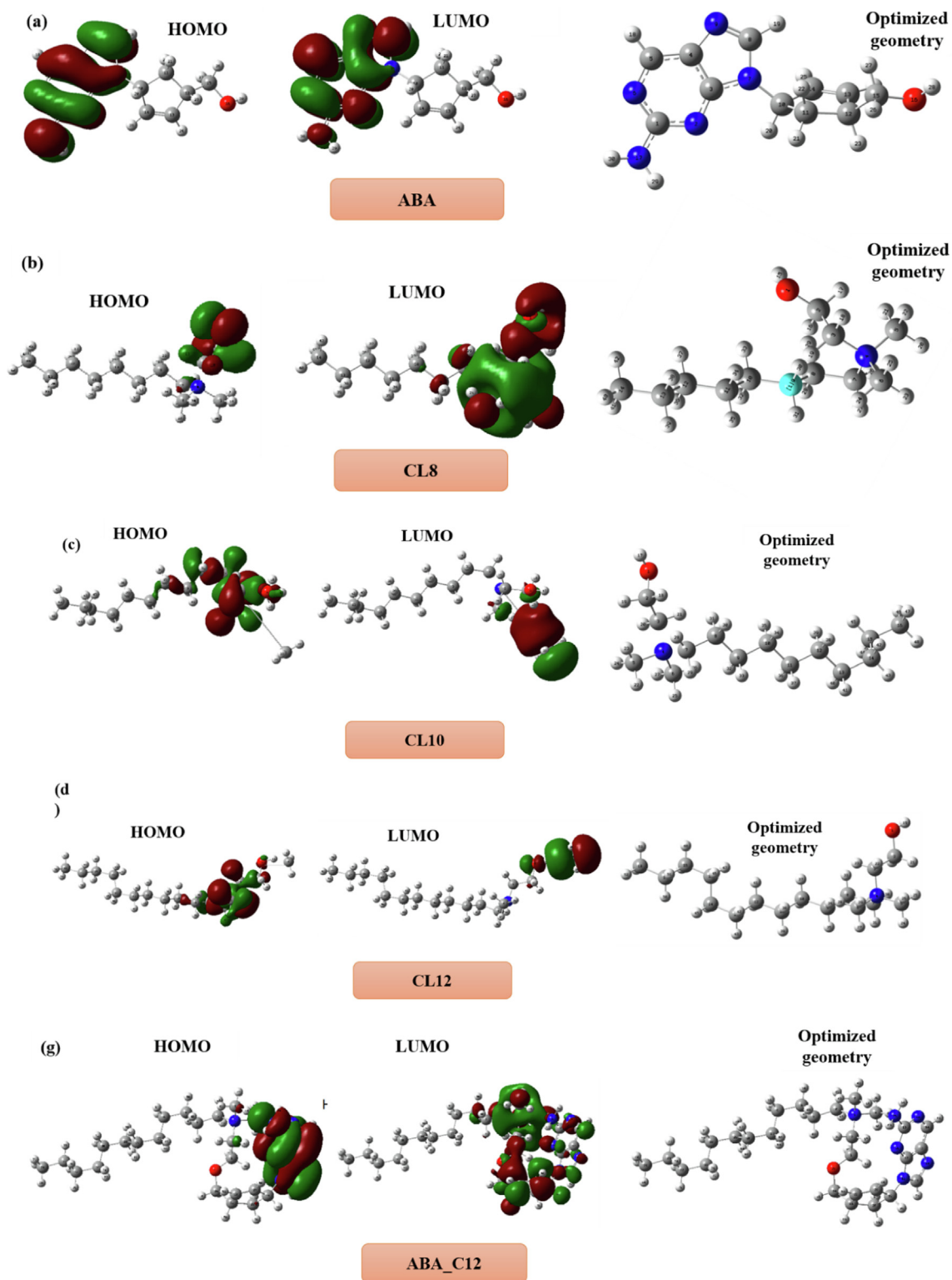


Fig. 6. Frontier molecular orbitals (HOMO and LUMO) and optimized geometry of (a) ABA (b) CL8 (c) CL10 (d) CL12 (e) ABA_CL8 (f) ABA_CL10 (g) ABA_CL12.

of the HOMO and LUMO, respectively ²¹. Further, E_{HOMO} and E_{LUMO} energy values obtained from DFT calculations as listed in Table 5 were used to calculate different physicochemical parameters viz. global electrophilicity index (ω), electronegativity (χ), chemical potential (μ), softness (S), and chemical hardness (η), respectively using Eqs. (1)–(5).

The popularity of DFT applications to elucidate the broad range of problems in pharmaceutical and biochemical interest has been growing rapidly, especially the interactions of candidate molecules such as drug-drug [36], drug-ionic liquids [37]. To understand the reactivity of the molecules, the physicochemical parameters obtained from DFT calculation plays an important

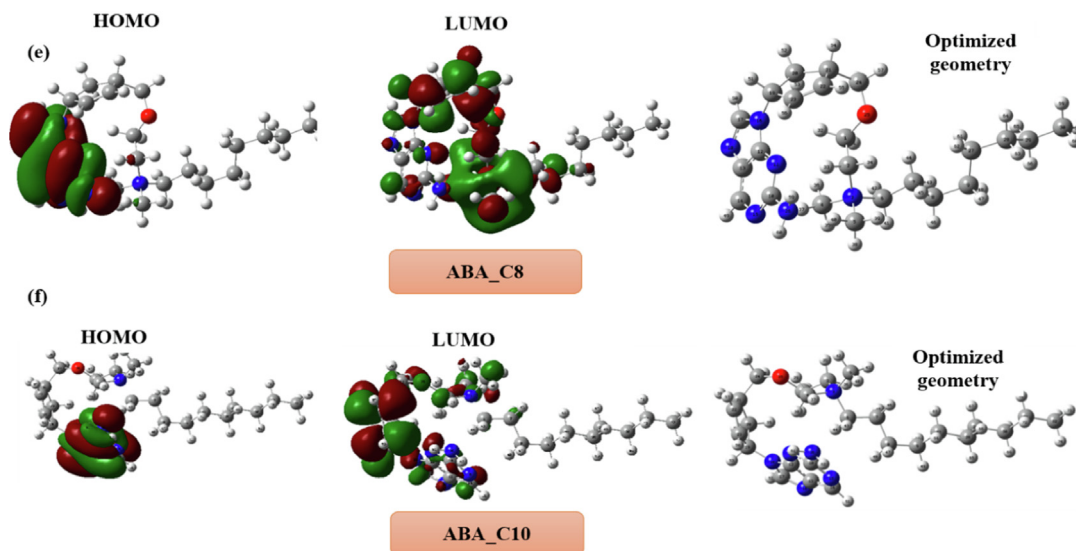


Fig. 6 (continued)

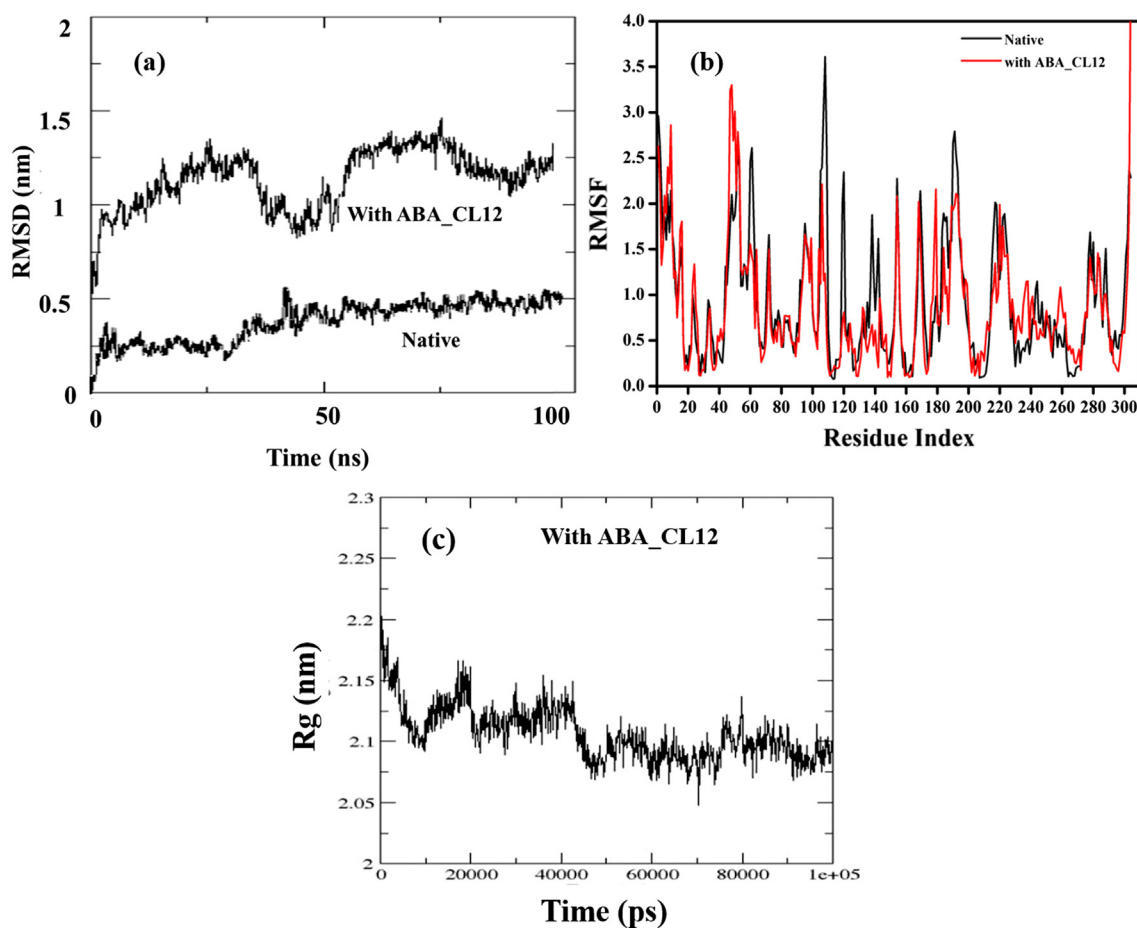


Fig. 7. (a) Root mean square deviation of the backbone atoms of the protein and docked complex (b) Root mean square fluctuation of the backbone atoms of the protein and docked complex (c) Radius of gyration of the complex generated from 100 ns MD simulations trajectory.

role. As per the reported literature, HOMO behaves as the electron donor while LUMO behaves as acceptor of electron [38]. The difference between the HOMO and LUMO energy level (ΔE_{H-L}) reveals the reactivity of the studied molecule. On moving

from CL8 to CL12 with ABA, the negative value of E_{H-L} increases and hence the stability of the complex increases. Therefore, system ABA_CL8, ABA_CL10, ABA_CL12 comes out to be most stable as depicted from the Table 5.

Table 5
Physiochemical descriptors of the ILs and ILs-AVDs system mentioned.

Parameters	ABA	CL8	CL10	CL12	ABA_CL8	ABA_CL10	ABA_CL12
E_{LUMO}	-0.027	0.067	0.07	0.08	0.028	0.027	0.025
E_{HOMO}	-0.207	-0.197	-0.184	-0.183	-0.237	-0.235	-0.243
$E_{HOMO}-E_{LUMO}$	-0.18	-0.264	-0.254	-0.263	-0.265	-0.262	-0.268
$E_{HOMO} + E_{LUMO}$	-0.234	-0.13	-0.114	-0.103	-0.209	-0.208	-0.218
Chemical hardness (η)	-0.0115	0.067	0.07	0.08	0.028	0.027	0.025
Electronegativity (χ)	0.117	0.065	0.057	0.0515	0.1045	0.104	0.109
Softness(S)	-43.478	7.462	7.142	6.25	17.857	18.518	20
Chemical potential (μ)	-0.117	-0.065	-0.057	-0.0515	-0.1045	-0.104	-0.109
Global electrophilicity index(ω)	-0.595	0.031	0.023	0.016	0.195	0.200	0.237
Dipole moment (Debye)	4.114	1.104	1.543	1.672	13.406	13.352	13.240
Point group	C1	C1	C1	C1	C1	C1	C1
Energy of the optimized structures	-775.964	-604.022	-682.470	-761.080	-1303.52	-1382.150	-1460.360

3.8. Molecular dynamic simulation

MD simulation was performed to evaluate the stability of target protein and screened conjugate. It also helped in determining any induced change in the protein by conjugate [39,40]. The RMSD profile of docked complexes for the best obtained conjugate and target protein was obtained using Webgro server as shown in Fig. 7. The trajectories of generated simulation run were analysed using RMSF and RMSD calculations. From MD simulations results, RMSF of screened best complex with coronavirus protease was analysed using CPPTRAJ module at 100 ns time period [41]. The RMSD of the protein backbone was consistent after 50 ns. In case of ABA_CL12-protease complex, the protein backbone RMSD stabilized after 80 ns as shown in Fig. 7a. The overall result suggests that after 80 ns the complex was stable. The amino acids contribute for the formation of the complex between main protease with the ABA_CL12 and showed structural fluctuations [42]. RMSF helps in determining the flexibility of each amino acid or the residue in the protease of the complex. The amino acids surrounding the ABA_CL12, showed fluctuations but was less as compared to the complex as in Fig. 7b. The RMSF value for complex of main protease of novel coronavirus was found to be 0.75–3.75 at 300 K, while RMSF value of complex with ABA_CL12 was found to be 0.51–3.25 at 300 K. The maximum fluctuation was seen at 80–120 positions. The lower fluctuations thereafter with RMSF value indicating more stability with a pronounced role of these residues in interaction. Rg results indicated that the compactness of the complex increases as Rg value found to be decreasing with time from 2.2 ns to 2.1 ns as shown in Fig. 7c. This confirms that point mutation in the conserved site caused structural stability leading to the increasing protein compactness [43].

4. Discussion

SARS-CoV-2 (COVID-19) pandemic is still a major health threat even after first wave in India. The second wave is much devastating as compared to first wave [44]. The delta variant is much more dangerous as that of β variant which was found responsible for first wave. Delta variant transmission was in fact much faster as that of β variant [45]. Though we have number of vaccine available to combat Covid-19 infection, but no such evidence has been seen showing the complete cure [10,12,46]. Therefore, we need to develop new effective drugs on urgent bases against novel SARS-CoV2. The combination therapy is always been a successful attempt in treating various threatful diseases [47,48]. The repurposing of the AVDs can potentially reduce the time and shortens the cost involved in drug discovery and clinical trials.

Recently, Kumar *et al.* has shown the conjugates of noscapine with various antiviral drugs such as Chloroquine, Hydroxychloro-

quine, Umifenovir, Favipiravir, and Galidesivir. They depicted the stability of the conjugates and revealed the improved drug accession along with the inhibitory regulation of the Mpro protein [49]. Magagnoli *et al.* worked with the conjugates of hydroxychloroquine and azithromycin, the study lacks in explaining the serious issues related with the high mortality rate and irregular heartbeat [50]. In our earlier publication, we explored the application of ILs as an antiviral agent computationally where we concluded the application of ILs as an antiviral agent [5]. The reason of being concern while working with ILs is their toxicity. As earlier reported, imidazolium, pyrrolidinium, pyridinium-based ILs are toxic [51]. Therefore, in the present study we focused on the known greener, non-toxic choline based ILs. Also, ILs hold many fascinating features with them such as tunability, liquid at room temperature, low vapour pressure, biological activity, etc [52,53]. The tunable characteristics of ILs make them a perfect class of compound where it can be designed on the basis of the application needed for [52]. We planned the repurposing of available antiviral drug by designing conjugates originating from (AVDs, ABA, ACY, and GAL) and choline-based ILs. The ABA, ACY and GAL are the known antiviral drugs active against novel coronavirus (details given in Table 1). The results showed the antiviral activity of choline based ILs against SARS-CoV2 virus. From Table 2, it was observed that with increasing the carbon chain length the binding energy with target protein increased suggesting the increasing antiviral activity with increasing hydrophobicity likewise the antibacterial activity as reported in our previous publications [15,16,54]. Further, the molecular docking results showed GAL > ABA > ACY order of antiviral activity of the drugs. The designed conjugates showed much increased activity as compared to AVDs and ILs alone. Best results in terms of least binding energy with target protein was shown by ABA_CL12 > ABA_CL10 > ABA_CL8. Rest all other conjugates also showed much improved results as compared to corresponding drugs and ILs (alone). Also, with increasing hydrophobicity the binding energy increased in case of conjugates also suggesting a higher potential of the conjugates against SARS-CoV2 virus. Though lot of computational work has been done in screening of active drug molecule towards inhibiting the SARS-CoV2 viral strain, our present approach is not yet known. The ADME and toxicity results revealed that the screened molecules are non-toxic and biocompatible. Additionally, the DFT study was also performed to investigate the interaction and specifically the reactivity of the conjugates formed between drugs and ILs which revealed the stability of the screened complexes as reported in the literature [55]. In the end, amongst the screened complexed; the complex with highest binding affinity was tested for the stability after binding with the target protein using molecular dynamic simulation. MD simulation results revealed that ABA_CL12 forms the stable complex once it gets bound to the target protein and

can therefore, act as an inhibitor of the Mpro protein leading to the prevention of entering of virus protein into the host cell [43].

5. Conclusion

In the present study, we have explored the new conjugation of antiviral drugs (abacavir, acyclovir, and Galdesivir) with choline-based ILs using computational approach. The blind docking of individual drug, ILs and IL-AVDs (conjugates) was done against SARS-CoV2 M_{pro} protease. Molecular docking results revealed the definite binding of AVDs, ILs and their conjugates with M_{pro} protease. Choline-based ILs are less toxic ILs as reported in the literature and with increasing carbon chain, the antiviral activity of ILs increased depicting that the ILs with highest hydrophobicity possess higher affinity towards Mpro protease. Though all the conjugates of drug and ILs showed improved binding affinity as compared to their corresponding drug and IL, however, the conjugates ABA and ILs showed the maximum binding with M_{pro} at the active site. Also, the hydrophobicity order was also seen in case of conjugates, with long carbon chain it showed maximum binding with M_{pro}. On the basis of maximum binding affinity (best fit molecules), three conjugates were screened out, ABA_CL12, ABA_CL10_ABA_CL8. ADME and toxicity results of screened molecule showed the compatibility of the molecule. Further, MD simulation results revealed that ABA_CL12 forms the stable complex once it gets bound to the target protein. Present study might help in boosting the current medication advancement against SARS-CoV2. Also, the inhibitory action of the drug in combination with ILs may lead to develop the new therapeutic agents which can contribute in combating the pandemic caused due to COVID-19 with conserving time in screening of molecule, cost reduction in failure trials. Moreover, these conjugates might be used as a potential antiviral agent but before any clinical application of these molecules detailed *in-vivo* and *in-vitro* studies would be needed in future to validate the findings.

Author Contributions

JS performed the whole work and wrote the manuscript.

UR performed the DFT calculation in the study.

RP is the overall corresponding author.

Declaration of Competing Interest

The authors declare that they have no known competing financial interests or personal relationships that could have appeared to influence the work reported in this paper.

Acknowledgements

Dr. Rajan Patel greatly acknowledges the financial support from Science and Engineering Research Board (EEQ/2020/000437) New Delhi, India.

Appendix A. Supplementary material

Supplementary data to this article can be found online at <https://doi.org/10.1016/j.molliq.2022.119277>.

References

- [1] J. Phua, L. Weng, L. Ling, M. Egi, C.-M. Lim, J.V. Divatia, B.R. Shrestha, Y.M. Arabi, J. Ng, C.D. Gomersall, *Lancet Respir. Med.* 8 (2020) 506.
- [2] W.H. Organization, (2021).

- [3] S. Iftimie, A.F. López-Azcona, I. Vallverdú, S. Hernández-Flix, G. De Febrer, S. Parra, A. Hernández-Aguilera, F. Riu, J. Joven, N. Andreychuk, *PLoS ONE* 16 (2021) e0248029.
- [4] M.A. Shereen, S. Khan, A. Kazmi, N. Bashir, R. Siddique, *J. Adv. Res.* (2020).
- [5] J. Saraswat, P. Singh, R. Patel, *Journal of Molecular Liquids* 115298.
- [6] M.S. Dhar, R. Marwal, V. Radhakrishnan, K. Ponnusamy, B. Jolly, R.C. Bhojar, S. Fatihi, M. Datta, P. Singh, U. Sharma, *medRxiv* (2021).
- [7] E. Boehm, I. Kronig, R.A. Neher, I. Eckerle, P. Vetter, L. Kaiser, *Clin. Microbiol. Infect.* (2021).
- [8] J.P. Sahoo, L. Ghosh, K.C. Samal, *Biotica Res. Today* 3 (2021) 273.
- [9] K.M. Agarwal, S. Mohapatra, P. Sharma, S. Sharma, D. Bhatia, A. Mishra, *Sensors Int.* (2020) 100037.
- [10] S. Kushwaha, A. Chakrabarty, U.S. Das, *Eur. J. Mol. Clin. Med.* 7 (2021) 6441.
- [11] M. Goyal, N. Tewatia, H. Vashisht, R. Jain, S. Kumar, *J. Infection Public Health* (2021).
- [12] D.-G. Ahn, H.-J. Shin, M.-H. Kim, S. Lee, H.-S. Kim, J. Myoung, B.-T. Kim, S.-J. Kim, *J. Microbiol. Biotechnol.* 30 (2020) 313.
- [13] B. Vellingiri, K. Jayaramayya, M. Iyer, A. Narayanasamy, V. Govindasamy, B. Giridharan, S. Ganesan, A. Venugopal, D. Venkatesan, H. Ganesan, *Sci. Total Environ.* (2020) 138277.
- [14] H.M. Wahedi, S. Ahmad, S.W. Abbasi, *J. Biomol. Struct. Dyn.* (2020) 1.
- [15] J. Saraswat, B. Aldahmash, S.Y. AlOmar, K. Imtiyaz, M.M.A. Rizvi, R. Patel, *Appl. Microbiol. Biotechnol.* (2020) 1.
- [16] J. Saraswat, F.A. Wani, K.I. Dar, M.M.A. Rizvi, R. Patel, *ACS omega* (2020).
- [17] K. Behera, P. Dahiya, S.J.o.c. Pandey, *i. science*, 307 (2007) 235.
- [18] J. Qin, J. Guo, Q. Xu, Z. Zheng, H. Mao, F. Yan, *ACS Appl. Mater. Interfaces* 9 (2017) 10504.
- [19] J. Saraswat, P. Singh, R. Patel, *J. Mol. Liq.* 326 (2021) 115298.
- [20] K. Palanisamy, S.E. Rubavathy, M. Prakash, R. Thilagavathi, M.S. Hosseini-Zare, C.J.R.A. Selvam, 12 (2022) 3687.
- [21] M. Musiał, A.B. Olejniczak, M. Denel-Bobrowska, E. Zorębski, M.J.A.S.C. Dzida, *Engineering* 9 (2021) 16459.
- [22] A. Trivedi, S. Sharma, B. Ashtey, *Pharma J.* (2020).
- [23] R. Hamza, T. Al-Talhi, A. Gobouri, W. Al-Sanie, S. El-Megharbel, *Adv. Anim. Vet. Sci* 9 (2021) 549.
- [24] P. Pandey, F. Khan, A.K. Rana, Y. Srivastava, S.K. Jha, N.K. Jha, *Biointerface Res. Appl. Chem* 11 (2021) 8482.
- [25] A.A. Elfiky, *Life Sci.* 253 (2020) 117592.
- [26] M. Moosavi, N. Banazadeh, M. Torzkadeh, *J. Phys. Chem. B* 123 (2019) 4070.
- [27] U. Norinder, C.A. Bergström, *ChemMedChem: Chem. Enabling, Drug Discovery* 1 (2006) 920.
- [28] P. Banerjee, A.O. Eckert, A.K. Schrey, R. Preissner, *Nucleic Acids Res.* 46 (2018) W257.
- [29] WebGRO for Macromolecular Simulations, <https://simlab.uams.edu/>.
- [30] A. Kuriata, A.M. Gierut, T. Oleniecki, M.P. Ciemny, A. Kolinski, M. Kurcinski, S.J. N.a.r. Kmiecik, 46 (2018) W338.
- [31] V.K. Vishvakarma, M.B. Singh, P. Jain, K. Kumari, P.J.A.a. Singh, 54 (2022) 205.
- [32] R.S. Tumskiy, A.V.J.C.P.L. Tumskaia, 780 (2021) 138894.
- [33] D. Butina, M.D. Segall, K.J.D.d.t. Frankcombe, 7 (2002) S83.
- [34] A.B. Raies, V.B.J.W.I.R.C.M.S. Bajic, 6 (2016) 147.
- [35] S.A. Ahmed, A.A. Rahman, K.N. Elsayed, H. Abd El-Mageed, H.S. Mohamed, S.A. Ahmed, *J. Biomol. Struct. Dyn.* (2020) 1.
- [36] M.J. Hoque, A. Ahsan, M.B.J.B.J.o.S. Hossain, T. Research, 9 (2018) 7360.
- [37] A. Kumar, K. Kumari, A.P.S. Raman, P. Jain, D. Kumar, P.J.J.o.P.O.C. Singh, 35 (2022) e4287.
- [38] M. Usman, F. Arjmand, M. Ahmad, M.S. Khan, I. Ahmad, S.J.I.C.A. Tabassum, 453 (2016) 193.
- [39] S. Ahmad, H.W. Abbasi, S. Shahid, S. Gul, S.W. Abbasi, *Dynamics* 39 (2021) 4225.
- [40] D. Kumar, K. Kumari, V.K. Vishvakarma, A. Jayaraj, D. Kumar, V.K. Ramappa, R. Patel, V. Kumar, S.K. Dass, R. Chandra, *Dynamics* 39 (2021) 4671.
- [41] H.M. Wahedi, S. Ahmad, S.W. Abbasi, *Dynamics* 39 (2021) 3225.
- [42] S. Borkotoky, M. Banerjee, *Dynamics* 39 (2021) 4111.
- [43] B. Pandey, A. Grover, P.J.B.g. Sharma, 19 (2018) 1.
- [44] D. Planas, D. Veyer, A. Baidaliuk, I. Staropoli, F. Guivel-Benhassine, M.M. Rajah, C. Planchais, F. Porrot, N. Robillard, J. Puech, *Nature* 596 (2021) 276.
- [45] P. Yadav, G.N. Sapkal, P. Abraham, R. Ella, G. Deshpande, D.Y. Patil, D. Nyayanit, N. Gupta, R.R. Sahay, A.M. Shete, *bioRxiv* (2021).
- [46] M.A. Yu, A.K. Shen, M.J. Ryan, L.L. Boulanger, *Bull. World Health Organ.* 99 (2021) 171.
- [47] K. Abdul Ghaffar, W.M. Hussein, Z.G. Khalil, R.J. Capon, M. Skwarczynski, I. Toth, *Curr. Drug Deliv.* 12 (2015) 108.
- [48] S. Dosler, A.A. Gerceker, *Chemotherapy* 57 (2011) 511.
- [49] N. Kumar, A. Awasthi, A. Kumari, D. Sood, P. Jain, T. Singh, N. Sharma, A. Grover, R. Chandra, *J. Biomol. Struct. Dyn.* (2020) 1.
- [50] J. Magagnoli, S. Narendran, F. Pereira, T.H. Cummings, J.W. Hardin, S.S. Sutton, *J. Ambati, Med* 1 (2020) 114.
- [51] A. Latała, M. Nędzi, P. Stepnowski, *Green Chem.* 11 (2009) 1371.
- [52] A.R. Bhat, F.A. Wani, K.A. Alzahrani, A.A. Alshehri, M.A. Malik, R. Patel, *J. Mol. Liq.* (2019) 111347.
- [53] R. Patel, J. Saraswat, *J. Mol. Liq.* (2021) 116844.
- [54] M.A. Siddiquee, J. Saraswat, K. Imtiyaz, A.R. Bhat, F.A. Wani, A.M. Alanazi, A.A. Khan, M.M.A. Rizvi, R. Patel, *J. Mol. Liq.* (2020) 115125.
- [55] S.B. Novir, M. Aram, *Chem. Phys. Lett.* 757 (2020) 137869.